

Deblurring 3D Characteristics of Heavy-Ion Collisions

Pawel Danielewicz*

*Facility for Rare Isotope Beams and Department of Physics and Astronomy,
Michigan State University, East Lansing, Michigan 48824, USA*

Mizuki Kurata-Nishimura

RIKEN Nishina Center, Hirosawa 2-1, Wako, Saitama 351-0198, Japan

(Dated: September 7, 2021)

Deblurring procedure is proposed for accessing three-dimensional (3D) differential distributions relative to the reaction plane in energetic high-multiplicity heavy-ion collisions. Because reaction plane direction can be only coarsely estimated in measurements for the collisions, any direct attempts to measure 3D characteristics will yield blurred results. However, it is not difficult to estimate the distribution of the estimated reaction plane direction around the true. Once that blurring function is known, a deblurring procedure can be applied to reveal underlying characteristics of the emission relative to the true reaction plane. This is similar to image restoration in optics, such as from an image recorded with a shaken camera.

Keywords: reaction plane; Richardson-Lucy algorithm; resolution

I. INTRODUCTION

Physics reach in a field can depend on availability of observables yielding detailed and simultaneously easily interpretable information. In heavy-ion collisions, any directional aspects of observables have been primarily tied to the incident beam direction, as in particular evidenced in the use of rapidity along the beam and/or transverse momentum magnitude in presenting data. However, the symmetry around the beam direction is broken in the initial state by the relative displacement of the nuclear centers, by impact parameter. The transverse displacement and the beam axis define the reaction plane for the collision. The symmetry breaking has important consequences for the collisions, such as in setting the preferred direction of transverse momentum transfer in the system and in the emergence of participant and spectator products in more energetic collisions. At lower energies, heavy projectile and target residues emerge from a collision largely aligned with the reaction plane and other characteristics of the final state tend to be related to these. At higher energies, much could be learned on reaction of strongly interacting matter to compression, from product emission in correlation to the reaction plane. However, at the same time, estimating the reaction plane becomes a challenge at those higher energies since the system largely vaporizes. Our considerations here will largely refer to the latter situation. At still higher energies, Lorentz dilation freezes fluctuations present the initial state, that can then compete with the breaking of the symmetry around the beam axis by the reaction plane. Even there our proposed methodology may have applications, though it might not provide the most interesting information one may there be after.

Correlation of particle emission pattern with the reaction plane can be exploited for estimating the direction of the reaction plane [1]. For low event statistics, transverse moments of the distributions can be evaluated. Because of the uncertainty in the reaction plane determination, values of the moments need to be renormalized, on a moment by moment basis, and this may be done in a self-consistent manner [1–4]. However, for high event statistics, the whole distribution associated with the reaction plane could be addressed [5]. With the uncertainty in the reaction plane determination, from one to another collision event, such a distribution is going to be smeared when evaluated directly. This is similar to the situation in optics where a photo is taken with a camera that shakes. For such situations and other, where distortions of image occur due to understood distortions of light intensity, deblurring techniques have been developed in the optical contexts [6].

We propose to use such techniques in the context of central heavy-ion collisions to arrive at three-dimensional (3D) distributions tied to the reaction plane. The interpretations of the latter distributions may be easier than of angular moments, especially those high, given that these moments tend to quantify information incidentally put together, through the reference to the same value of transverse momentum magnitude.

We start out by presenting a schematic one-dimensional (1D) example, where a system moving at unknown velocity emits particles according to a single-particle distribution that is forward-backward symmetric in the c.m. frame. A

* daniel@frib.msu.edu

number of particles is measured and the goal is to determine the velocity distribution of particles relative to the center of mass, even though the center of mass is not known on the case by case basis. The center of mass velocity may be estimated from the emitted particles, but it straggles relative to the true velocity. With this, the distribution relative to the center of mass evaluated from the emitted particles alone is smeared out compared to the true distribution. We demonstrate that the original distribution may be restored from the simulated observations by combining the central limit theorem with Richardson-Lucy deblurring algorithm [7, 8]. We next turn to simulated distributions for heavy-ion collisions. We assume a typical situation recognized as a good representation of the final-state emission for semicentral collisions at few hundred MeV/nucl, with a local equilibrium combined with sideward, radial and elliptic flows. With a moderate number of light charged particles registered, with mass $A \leq 4$, it is possible to deblur their distributions associated with the reaction plane, even when these distributions vary by an order of magnitude or more in the transverse directions. We complement the outline of the strategy for data analysis with results from transport theory, illustrating what kind of information could be accessed in the deblurred distributions, that might not be easily seen in the azimuthal moments for the distributions.

II. DEBLURRING

The blurring problem may be stated in the form of the equation:

$$n(\zeta) = \int d\xi P(\zeta|\xi) \mathcal{N}(\xi). \quad (1)$$

Here, $\mathcal{N}(\xi)$ is the distribution in coordinates ξ that faithfully characterizes the measured system and $P(\zeta|\xi)$ is the probability density that the system is measured around ζ when it is actually at ξ . Finally, $n(\zeta)$ is the distribution attributed to the system in effect of the direct measurements. The goal of deblurring is to determine $\mathcal{N}(\xi)$ from the measured $n(\zeta)$, given knowledge about P . While the problem appears stated as linear, in practical situations P may have a dependence on \mathcal{N} , too.

In the reaction-plane problem, the blurring is due to the fact that the azimuthal angle relative to the estimated reaction plane is not equal to the angle relative to the true reaction plane. The deviation may vary from one collision event to another and even particle to a particle, within the strategy of estimating the reaction plane orientation [1, 2]. In detector efficiency problems, P might account for particle being misidentified or missed or whole event disregarded consequently under a trigger. Depending on the situation, the probability density integrates to 1 or not, $\int_Z d\xi P(\zeta|\xi) = P_Z(\xi) \leq 1$.

For inferring \mathcal{N} directly from measured n , it might be tempting to invert (1) directly, but that strategy is likely to amplify short-wavelength noise always present in n . In optical contexts alternative methods have been developed of which the Richardson-Lucy (RL) deconvolution algorithm [7, 8], based on Bayesian considerations that we next lay out, is particularly popular.

Let $Q(\xi|\zeta)$ denote complementary probability density to P , that the system is at ξ when it is measured at ζ . Then the probability that the system is within $d\xi$ while measured within $d\zeta$ can be expressed in two different ways:

$$Q(\xi|\zeta) n(\zeta) d\zeta d\xi = P(\zeta|\xi) \mathcal{N}(\xi) d\xi d\zeta. \quad (2)$$

This yields

$$Q(\xi|\zeta) = \frac{P(\zeta|\xi) \mathcal{N}(\xi)}{\int d\xi' P(\zeta|\xi') \mathcal{N}(\xi')}, \quad (3)$$

and

$$\mathcal{N}(\xi) = \frac{\int d\zeta Q(\xi|\zeta) n(\zeta)}{P_Z(\xi)}. \quad (4)$$

The RL method solves the last two equations iteratively:

$$Q^{(r)}(\xi|\zeta) = \frac{P(\zeta|\xi) \mathcal{N}^{(r)}(\xi)}{\int d\xi' P(\zeta|\xi') \mathcal{N}^{(r)}(\xi')}, \quad (5)$$

$$\mathcal{N}^{(r+1)}(\xi) = \frac{\int d\zeta Q^{(r)}(\xi|\zeta) n(\zeta)}{P_Z(\xi)}, \quad (6)$$

where r is iteration step index. Any implicit dependence of P on \mathcal{N} may be handled in the equations iteratively. One notable feature of the equations is that distributions that start as nonnegative stay such during the iterations. Combination of the equations above yields

$$\mathcal{N}^{(r+1)}(\xi) = A^{(r)}(\xi) \cdot \mathcal{N}^{(r)}(\xi), \quad (7)$$

where

$$A^{(r)}(\xi) = \frac{\int d\zeta P(\zeta|\xi) \frac{n(\zeta)}{n^{(r)}(\zeta)}}{\int d\zeta' P(\zeta'|\xi)}, \quad (8)$$

and

$$n^{(r)}(\zeta) = \int d\xi P(\zeta|\xi) \mathcal{N}^{(r)}(\xi). \quad (9)$$

If the variable space is discretized, then the equations become

$$\mathcal{N}_i^{(r+1)} = A_i^{(r)} \cdot \mathcal{N}_i^{(r)}, \quad (10)$$

$$A_i^{(r)} = \sum_j P_{ji} \frac{n_j}{n_j^{(r)}} \Big/ \sum_{j'} P_{j'i}, \quad (11)$$

and

$$n_j^{(r)} = \sum_i P_{ji} \mathcal{N}_i^{(r)}. \quad (12)$$

When n and \mathcal{N} extend over the same domain, it is common to use n to start the iterations for \mathcal{N} . It is common for the iterations to progress quickly first, but then gradually stall, with seesaw instabilities developing over many iterations. Remedies include an acceleration [9] by using a power $\nu > 1$ for the amplification factor A , terminating the iterations after a moderate number of steps, and/or using a regularization factor [9, 10]:

$$I^{(r)} = \frac{1}{1 - \lambda \mathbf{H} \cdot \nabla (\nabla \mathcal{N}^{(r)}) / |\nabla \mathcal{N}^{(r)}|}. \quad (13)$$

Here, \mathbf{H} is the discretization vector within the domain of \mathcal{N} and λ is a small factor that prevents build-up of any seesaw pattern in effect of the iterations. I.e., Eq. (10) can be replaced with

$$\mathcal{N}_i^{(r+1)}(\xi) = [A_i^{(r)}(\xi)]^\nu \cdot I_i^{(r)} \cdot \mathcal{N}_i^{(r)}(\xi), \quad (14)$$

in an accelerated regularized LR scheme. Excessive acceleration powers, $\nu > 2$, have been shown to lead to an instability on its own in the iterations.

Obviously other methods of inferring n from \mathcal{N} are possible, such as in decomposing them in orthogonal functions, including harmonics [3, 5]. The danger in the latter case is of combining functions with varying sign where noise is handled independently. In the case of functions that change by orders of magnitude, the danger is of arriving at a poorer representation for \mathcal{N} in the regions of low values than even provided by n .

III. 1D MODEL

We next present a schematic 1D model that is easy to see through. It may seem at first disconnected from the issue of reaction-plane deblurring. In reality, it is closely related.

We consider a projectile moving at an unknown velocity V_0 that varies from an event to an event. The projectile de-excites emitting $N = 10$ identical particles sampled from a uniform velocity distribution from -1 to +1 relative to V_0 , in some arbitrary velocity units. The particle velocities are measured and the goal is to determine, from event statistics, the distribution of particles in the projectile frame. For uncorrelated emission, the rms of the sought distribution is obviously easy to estimate from the average difference of velocities between any two particles squared:

$$\langle (v_1^{\text{lab}} - v_2^{\text{lab}})^2 \rangle = \langle (v_1 - v_2)^2 \rangle = 2\langle v^2 \rangle. \quad (15)$$

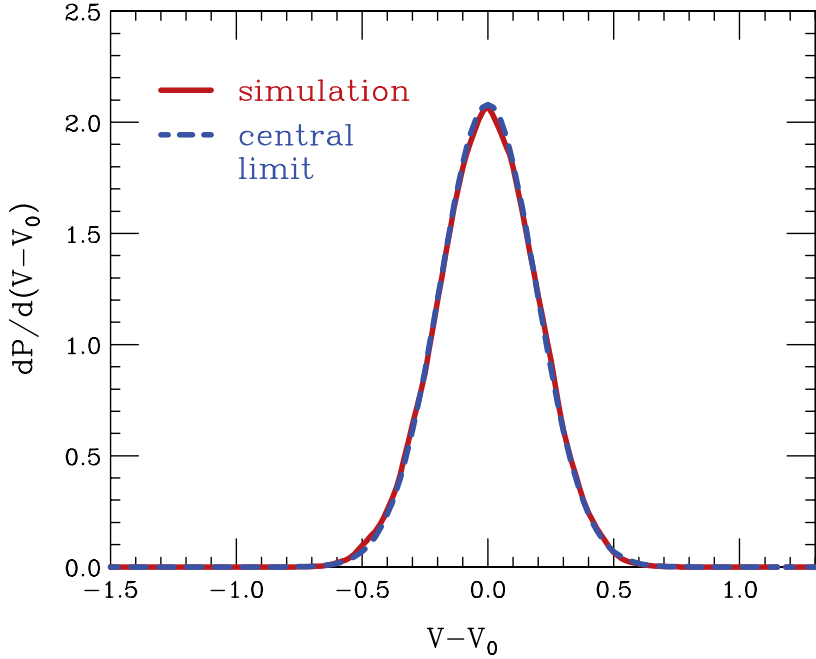


FIG. 1. Probability density for system velocity V , estimated with the average velocity for $N - 1 = 9$ particles sampled from a symmetric uniform velocity distribution centered around the true velocity V_0 . The solid (red) line shows the distribution from a direct simulation, calculated with $H = 0.1$ binning, and the dashed (blue) line - the distribution estimated with the central-limit theorem.

Here, v are velocities relative to the projectile and v^{lab} are in the laboratory system: $v^{\text{lab}} = v + V_0$.

In assessing velocity of a particle relative to the projectile, the velocity of the projectile can be estimated with the average velocity of $N - 1 = 9$ remaining particles, in a similar manner as when reaction plane is estimated from remaining particle in an event [1]. The so assessed velocity V fluctuates though around the true velocity V_0 . The probability distribution from simulated 10,000 events is shown as a solid curve in Fig. 1. The central-limit theorem states that for a large particle number in one event such a distribution approaches a Gaussian

$$\frac{dP}{dV} \simeq \sqrt{\frac{(N-1)}{2\pi\langle v^2 \rangle}} \exp\left[-\frac{(N-1)(V-V_0)^2}{2\langle v^2 \rangle}\right]. \quad (16)$$

We compare that Gaussian distribution to the one from simulations and it is apparent that the two distributions are nearly indistinguishable in the region where they are significant.

Because of the fluctuations of the reference V , around the true velocity V_0 , the inferred velocities v' relative to the projectile are inaccurate, $v' = v + V_0 - V$, and the inferred distribution in velocity gets smeared out:

$$\frac{dN}{dv'}(v') = \int dV \frac{dP}{dV}(V - V_0) \frac{dN}{dv}(v). \quad (17)$$

In Fig. 2, we show the original distribution of particles relative to the projectile in the simulations, together with that from simulated measurements and the smearing is evident. In collecting the statistics, we use $H = 0.1$ bin size. The third distribution represented in Fig. 2 is one from deblurring using the regularized and accelerated RL algorithm. In 1D, the regularization factor is

$$I_i^{(r)} = \begin{cases} \frac{1}{1-\lambda}, & \text{if } \mathcal{N}_i^{(r)} < \mathcal{N}_{i-1,i+1}^{(r)}, \\ \frac{1}{1+\lambda}, & \text{if } \mathcal{N}_i^{(r)} > \mathcal{N}_{i-1,i+1}^{(r)}, \\ 1, & \text{otherwise.} \end{cases} \quad (18)$$

We employ $\lambda = 0.01$ and accelerating power $\nu = 1.99$ and start with $\mathcal{N}^{(1)} = n$. Moreover, we carry out the iterations in (14) by using the central-limit blurring function (16) with (15). In principle, it could be possible to update the blurring functions during iterations to make it consistent with the inferred dN/dv , for finite N , if desired accuracy of restoration called for that. At the level of the statistics we employ, the iterations that employ our more basic procedure stabilize at a distribution that is largely consistent with the original.

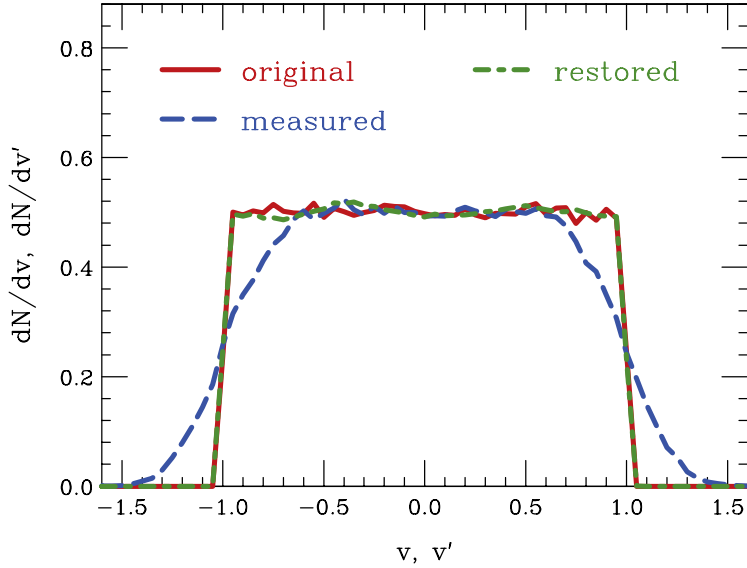


FIG. 2. Distribution of particles in velocity within the projectile frame for 1D model: original represented by the solid (red) line, inferred from measurements represented by the dashed (blue) line and restored through deblurring and represented by the dash-dot (green) line. In the simulation, 10,000 of events with $N = 10$ particles each were generated. A binning of $H = 0.1$ was used for the distributions. The restoration was done assuming the central-limit blurring function.

IV. REACTION-PLANE DEBLURRING

The problem of the blurring of particle distributions and other characteristics of heavy-ion collisions lies in attributing azimuthal angle Φ to the reaction plane that is actually directed at angle Φ_0 . With this, the angles relative to the reaction plane attributed to the particles are inaccurate, $\phi' = \phi + \Phi_0 - \Phi$, and measured distributions are going to be smeared out:

$$\frac{d^3 N}{p_\perp dp_\perp dy d\phi'} = \int d\Phi \frac{dP}{d\Phi}(\Phi - \Phi_0) \frac{d^3 N}{p_\perp dp_\perp dy d\phi}(\phi). \quad (19)$$

Owing to the asymmetries in emission tied with the reaction plane, the direction of the reaction plane is estimated with a combination of particle momenta, most commonly sum of weighted transverse momenta, $\mathbf{q}_\nu = \omega_\nu \mathbf{p}_{\perp\nu}$. When the direction of the reaction plane is used as a reference for a certain particle μ , that particular particle is omitted from the reference, to avoid a self-correlation. I.e., the reaction plane direction is estimated with the direction of the vector [1, 11]

$$\mathbf{Q}_{\mu'} = \sum_{\nu \neq \mu} \omega_\nu \mathbf{p}_{\perp\nu} = \sum_{\nu \neq \mu} \mathbf{q}_\nu. \quad (20)$$

The direction is obviously the same as for the average vector \mathbf{q} of the remaining particles

$$\overline{\mathbf{q}_{\mu'}} = \frac{1}{N-1} \sum_{\nu \neq \mu} \mathbf{q}_\nu, \quad (21)$$

where N is particle multiplicity. When \mathbf{q}_ν are largely uncorrelated, except through the reaction-plane geometry, the central-limit theorem implies the distribution of the average vector $\overline{\mathbf{q}}$ in relation to the reaction plane approaches Gaussian for large N :

$$\frac{d^2 P}{d^2 \overline{q}} \simeq \frac{N-1}{2\pi \sigma_x \sigma_y} \exp \left\{ -\frac{N-1}{2} \left[\frac{(\bar{q}_x - \langle q_x \rangle)^2}{\sigma_x^2} + \frac{\bar{q}_y^2}{\sigma_y^2} \right] \right\}. \quad (22)$$

Here, index x is for a component along the reaction-plane direction and y – along the perpendicular direction. The dispersions σ and average $\langle q_x \rangle$ refer to single-particle emission in relation to the reaction plane,

$$\begin{aligned} \sigma_x^2 &= \langle (q_x - \langle q_x \rangle)^2 \rangle = \langle q_x^2 \rangle - \langle q_x \rangle^2, \\ \sigma_y^2 &= \langle q_y^2 \rangle, \end{aligned} \quad (23)$$

Under the condition that the correlations tied to the reaction plane dominate [12], the parameters for the probability distribution can be determined from constructs out of the \mathbf{q} contributions averaged over particle sets and events:

$$\begin{aligned}\langle \mathbf{q}_1 \cdot \mathbf{q}_2 \rangle &= \langle q_x \rangle^2, \\ \langle 2(\mathbf{q}_1 \cdot \mathbf{q}_2)(\mathbf{q}_2 \cdot \mathbf{q}_3) - (\mathbf{q}_1 \cdot \mathbf{q}_3) q_2^2 \rangle &= \langle q_x \rangle^2 (\langle q_x^2 \rangle - \langle q_y^2 \rangle).\end{aligned}\quad (24)$$

Here, the indices 1, 2 and 3 refer to any three particles contributing to \mathbf{Q} in an event.

Now, we can express $\bar{\mathbf{q}}$ in terms of azimuthal deviation from the true direction of the reaction plane, $\Delta\Phi = \Phi - \Phi_0$

$$\bar{q}_x = \bar{q} \cos \Delta\Phi, \quad \bar{q}_y = \bar{q} \sin \Delta\Phi, \quad (25)$$

and write the probability density (22) as

$$\frac{d^2 P}{d^2 \bar{q}} = \frac{d^2 P}{\bar{q} d\bar{q} d\Phi} \simeq \mathcal{A} \exp \left[-\mathcal{B}(\Delta\Phi) \bar{q}^2 + 2\mathcal{C}(\Delta\Phi) \bar{q} \right]. \quad (26)$$

Integration over magnitude of \bar{q} yields the central-limit distribution of the estimated reaction plane relative to the true plane:

$$\frac{dP}{d\Phi} = \int d\bar{q} \bar{q} \frac{d^2 P}{d^2 \bar{q}} \simeq \alpha(\Delta\Phi) \left\{ 1 + \sqrt{\pi} \beta(\Delta\Phi) \exp(\beta^2(\Delta\Phi)) [1 + \text{erf}(\beta(\Delta\Phi))] \right\}. \quad (27)$$

Here, the terms β and α , both dependent on the deviation $\Delta\Phi$ from the true reaction plane, are

$$\beta(\Delta\Phi) = \frac{\mathcal{C}(\Delta\Phi)}{\sqrt{\mathcal{B}(\Delta\Phi)}} = \sqrt{\frac{N-1}{2(\sigma_y^2 \cos^2 \Delta\Phi + \sigma_x^2 \sin^2 \Delta\Phi)}} \frac{\sigma_y}{\sigma_x} \langle q_x \rangle \cos \Delta\Phi \approx \sqrt{\frac{N-1}{\langle q^2 \rangle}} \langle q_x \rangle \cos \Delta\Phi. \quad (28)$$

and

$$\alpha(\Delta\Phi) = \frac{\mathcal{A}}{2\mathcal{B}(\Delta\Phi)} = \frac{\sigma_x \sigma_y \exp \left[-\frac{(N-1)\langle q_x \rangle^2}{2\sigma_x^2} \right]}{2\pi (\sigma_y^2 \cos^2 \Delta\Phi + \sigma_x^2 \sin^2 \Delta\Phi)} \approx \frac{1}{2\pi} \exp \left[-\frac{(N-1)\langle q_x \rangle^2}{\langle q^2 \rangle} \right], \quad (29)$$

see also Ref. [3]. The final approximations in Eqs. (28) and (29) pertain to the case of weak azimuthal anisotropies in the distributions relative to the reaction plane. These underscore that the main variation with angle in (27) is tied to the factor of $\cos \Delta\Phi$ in (28).

An example of the distribution (27) is shown in Fig. 4. We next illustrate the envisioned procedure of reaction plane deblurring in the case of the final state modelled using a local-equilibrium model that incorporates common concepts for intermediate-energy heavy-ion collisions.

A. Deblurring Example: Local-Equilibrium Model

We illustrate deblurring for a 3D distribution associated with the reaction plane, deducing $d^3 N / p_\perp dp_\perp dy d\phi$ from $d^3 N / p_\perp dp_\perp dy dy d\phi'$, c.f. Eq. (19), by simulating the final state of a collision in a local equilibrium model. As a reference beam energy for the collision, we take 300 MeV/nucl and consider $A \leq 4$ charged products in the final state.

Our goal is to mimic a state that is consistent at a very coarse level with the observations [11, 13]. We have no intention to dive into any controversies around the freeze-out in collisions, whether the colliding systems literally go through an equilibrium when expanding into vacuum or whether they separately freeze out chemically and kinematically. Specifically, we assume that the system freeze-out can be described in terms of a local equilibrium, at a uniform freeze-out density ρ_f and temperature T_f , combined with collective motion for the freeze-out location. Within the latter, the longitudinal expansion dominates, but also present are a radial transverse expansion, with a weak elliptical modulation, and finally a weak sideward flow, typical for mid-central collisions. We take the freeze-out density at $\rho_f = \rho_0/6$ and, for simplicity, a neutron-proton symmetric system. Assuming that the local kinetic energy for nucleons is a fraction of the kinetic energy available per nucleon, we arrive at the freeze-out temperature $T_f \simeq 29$ MeV. To fix the attention, we assume that the average number of protons included in the measurements, whether as free or in clusters, is $\langle Z_t \rangle = 50$. Then, ρ_f and T_f give us charged particle multiplicities, $\langle N_p \rangle = 19.0$, $\langle N_d \rangle = 17.8$, $\langle N_t \rangle = \langle N_h \rangle = 3.7$, and $\langle N_\alpha \rangle = 1.0$. The $A \geq 3$ multiplicities are low, for a given proton multiplicity, compared to the data from the specific beam energy region [13]. However, our main goal is to explore the situation with different

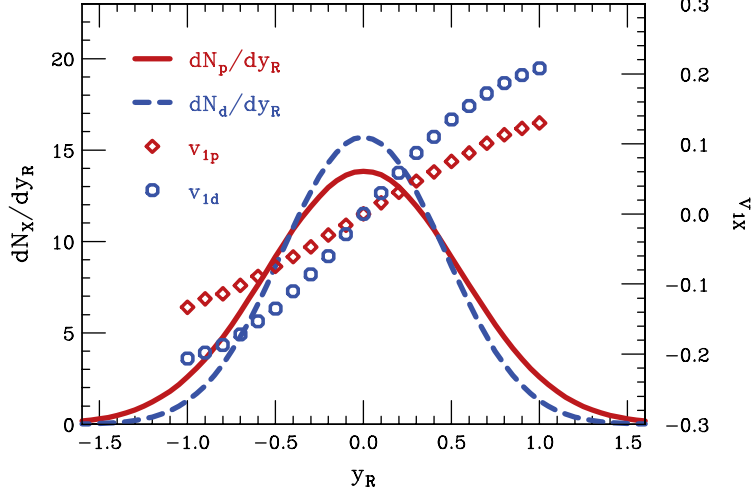


FIG. 3. Characteristics of protons and deuterons within the local equilibrium model. The lines represent differential distributions in normalized rapidity, dN_X/dy_R , and symbols represent first-order azimuthal-asymmetry coefficients, $v_{1X} = \langle \cos(\phi - \Phi_0) \rangle_X$, all vs y_R . Here, the rapidity is in the center of mass and scaled with the rapidity of the beam, $y_R = y/y_{\text{Beam}}$.

species used in reaction plane determination, not a literal reproduction of relative yield data. We sample multiplicities for the species from Poisson distributions for the average specie multiplicities and we combine a momentum sampled from a local equilibrium distribution for the specific species with a collective velocity boost that itself combines the aforementioned longitudinal persistence, radial transverse expansion and elliptic and sideward flows, all of the latter common between the species. In Fig. 3, we show exemplary characteristics of protons and deuterons in the generated events. Second-order coefficients of azimuthal anisotropy have low values in this simulation, in fact for protons quite comparable to statistical errors even for a large number of events, and are not shown.

In each of the events in the sample, when considering particle μ , we estimate the reaction plane direction with the remaining particles in the event. We use

$$\omega_\nu = \begin{cases} \text{sgn } y_R, & \text{if } |y_R| > \delta, \\ 0, & \text{if } |y_R| < \delta, \end{cases} \quad (30)$$

in Eq. (20), with $\delta = 0.17$ [1]. The distribution of estimated plane directions, relative to the true direction, is shown in Fig. 4 for this choice of weights. More optimal weights could be chosen, yielding a more narrow distribution [11, 14]. Our goal here, though, is of presenting deblurring opportunities and not of making of making everything optimal - actual experimental analysis will likely face other tensions. In addition to the distribution found in the simulations, we show in Fig. 4 the central-limit result (27), with widths from Eqs. (23) and (24), and N replaced by the average $\langle N \rangle$ for the simulation. Remarkably, the curves cannot be distinguished by eye, which bodes well for using central-limit results in practice, in lieu of any complete self-consistent simulation. Notably, testing of the proximity to the central-limit can be carried out directly in the experiment, by randomly dividing events into subevents of nearly equal multiplicity [1] and comparing the relative distribution of estimated directions of the reaction plane to that from Eq. (27) with $(N - 1)$ replaced by $\langle N \rangle/4$.

We next illustrate the blurring that occurs when attempting to measure the triple differential distribution. To the blurred distribution we apply deblurring. Specifically, we examine the spectrum of deuterons at a moderately forward rapidity, $y_R = 0.5$. We choose deuterons rather than protons in the illustration, because the push of the latter in the reaction plane is relatively meager in the parameterization of the flows we chose. Figure 5 shows three versions of the transverse momentum spectra in the reaction plane ($p_y = 0$): as recorded for the event sample using the known direction of the reaction plane (diamonds), as recorded (crosses) when using the direction estimated with a construct from particle momenta, Eqs. (20) and (21), and as obtained from deblurring the blurred spectrum (circles). The blurring function for the latter could be determined self-consistently, through additional simulations during the deblurring iterations, but given Fig. 4 we instead use the central-limit formula (27). The discretization step in the RL algorithm is the same for the blurring function and the distribution and we use $H = 15^\circ$. The values from restoration settle after about 5 RL iterations with $\nu = 1.99$ and $\lambda = 0.005$. The deblurring is carried out for each transverse momentum bin separately and the inset in Fig. 5 shows the case of a high central bin momentum, $p_\perp = 1.17 \text{ GeV}/c$, with statistical fluctuations evident.

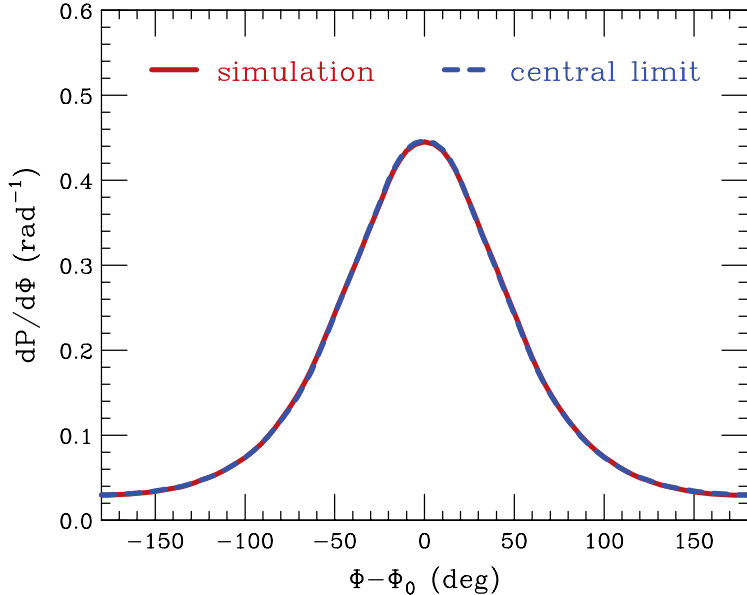


FIG. 4. Probability density for the azimuthal angle Φ of the reaction plane in the local equilibrium model, when estimated with the direction of the vector $\bar{\mathbf{q}}$ out of $N - 1$ particles in an event, relative to the true angle Φ_0 . Here, N is the total particle number in an event. The solid (red) line shows the density from a direct simulation in the local equilibrium model and the dashed (blue) line shows the density estimated with the central-limit Eq. (27). In using the last equation, $\langle q_x \rangle$, σ_x^2 and σ_y^2 in α and β were obtained from averages over the event simulations, following the strategy laid out in the text. In addition, the multiplicity N , actually varying from an event to event, was replaced with the single average value $\langle N \rangle$ over the simulated events.

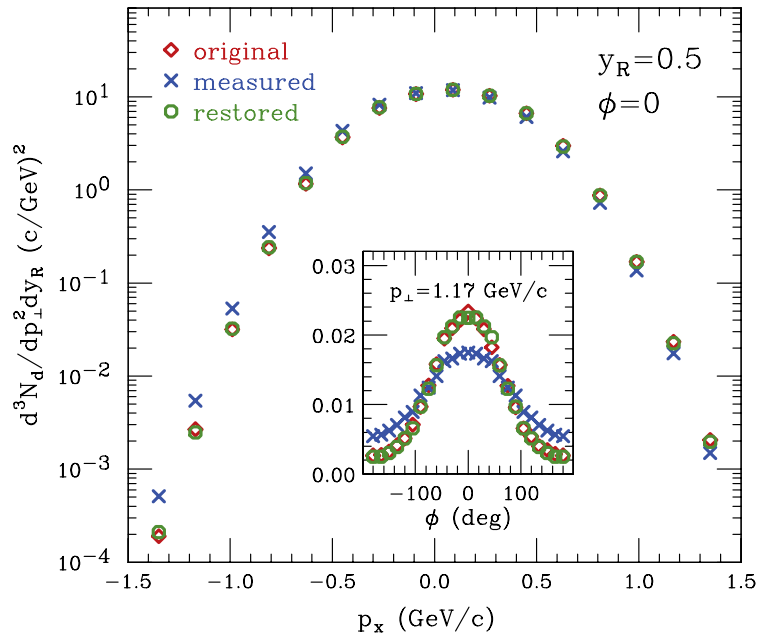


FIG. 5. Triple differential deuteron distribution at $y_R = 0.5$, in the local equilibrium model. The main figure shows the distribution in the reaction plane, as a function of the momentum component in the reaction plane. The inset shows the distribution at $p_\perp = 1.17 \text{ GeV}/c$, as a function of azimuthal angle about the reaction plane. In each case, three versions of the distribution are displayed: one determined directly using the known direction of the reaction plane in the modelled events (diamonds), one obtained by estimating the direction of the plane with the vector \mathbf{Q} (crosses), out of momenta of remaining particles in the simulated events, Eq. (20), and one arrived by applying the deblurring to the measured triple-differential distribution, with the RL algorithm applied to Eq. (19) and the blurring function from the central limit theorem, Eq. (27).

It is apparent in Fig. 5 that the restored spectrum well coincides with the original, as the respective representing symbols largely overlap. It is apparent, for the high momenta there, that the restoration can reproduce spectra varying by an order of magnitude over the azimuthal angle fine. Much of the variation over angle is already there in the simulated measured spectrum, see the inset. The restoration just improves details in that variation and does so mostly on a local scale in the azimuthal angle. Had we chosen different weights for \mathbf{Q} in Eq. (30), the blurring function in Fig. 4 could have been more narrow, and there would be less needed improvement left for the deblurring.

B. Why 3D Characteristics?

It may be asked why engage in deblurring, if procedures exist for determining azimuthal Fourier coefficients, as a functions of transverse momentum [4, 5]. The lowest nonvanishing coefficients usually have a straightforward physical meaning and may be easier to determine for low event statistics than refined distributions. However, a multitude of coefficients of different orders, changing with rapidity and transverse momentum, combining information from different azimuthal directions, can be a challenge at operational level. To illustrate how the view of reactions could be expanded by examining distributions that include azimuthal angle relative to the reaction plane, and potentially 3D distributions, we reach to the pBUU transport model [15]. The latter and other transport models have been extensively used to simulate a variety of heavy-ion collisions in the beam energy region from few tens of MeV/nucl to few GeV/nucl, describing different observables at quantitative and semi-quantitative level [16]. With this predictions of such models might be considered meaningful, but as azimuthal and more broadly 3D spectra have not been accessible experimentally, they were normally not considered in the theory either.

Multiple transport simulations have been carried out in the context of 270 MeV/nucl Sn + Sn experiments performed recently at RIKEN [17]. In Fig. 6, we show exemplary results from such simulations, proton and neutron spectra from $^{132}\text{Sn} + ^{124}\text{Sn}$ collisions at $b = 3.3\text{ fm}$, within the reaction plane at $y_R = 0.5$. With projectile and target of different mass, the rapidity is taken here in the nucleon-nucleon center of mass and is normalized to the beam. There are similarities and differences between the spectra in the conventional local equilibrium picture, such as in Fig. 5, and from transport, such as in Fig. 6, when the spectra are examined in the reaction plane. Both types of spectra have maxima shifted in the positive direction of the reaction plane. The one in the conventional picture is largely symmetric about the fairly flat maximum and close to parabolic in the logarithmic scale. The maxima in the spectra from transport are sharp, the spectra are largely piecewise exponential in momentum, have knees and there is visible asymmetry between the sides extending into the positive and negative sides of the reaction plane. The slope for the positive side, right after the maximum, is sharper than for the negative side. This could be due to a larger fraction of spectator matter towards the positive side of the reaction plane in space, for particles moving forward, than towards the negative. The knees in the spectra are at different transverse momenta on the two sides of the reaction plane. A sharp maximum could be produced by Coulomb interactions, but these cannot explain the maximum for neutrons, that seems to be even sharper than for protons.

When the transport spectra are averaged over azimuthal angle, the maxima in the spectra move to $p_{\perp} = 0$ and soften (smear?). The knees soften too. Overall, the two types of spectra, from transport and the conventional picture, become qualitatively much closer to each other with the azimuthal angle-averaging than without. When azimuthal asymmetries in the spectra are explored in terms of Fourier coefficients, usually just one or two lowest ones in the particular energy regime, details such as in Fig. 6 are beyond resolution.

Differences in the spectra for the sides of the system with different participant-spectator composition on different sides of the reaction plane may be accessible only through the 3D examination of those spectra. Shift of a maximum in the spectrum within the reaction plane may offer the only opportunity to examine its shape, as a maximum can be difficult to assess when it coincides with beam direction. Comparison of the knees in relation to the maximum, between experiment and theory may help to clarify their origin and clarify the level of understanding of the collisions within theory, such as of the elementary collisions taking place on shell.

Turning to the second example, heavy-ion collisions compress nuclear matter to densities above normal at conditions approaching thermal equilibrium. With this they represent opportunity to learn about the nuclear equation of state (EOS). The current interest is in the component of EOS, so-called symmetry energy that describes energy change with the change in relative neutron-proton asymmetry, at different net nucleonic densities. Energies of more massive nuclei, and other data, constrain the symmetry energy at subnormal densities and especially at the density representing an average for the nuclei, $\rho \simeq 2\rho_0/3$, at a value of about 25.4 MeV [18]. With that, the uncertainty in the symmetry energy becomes the pace of density variation when passing near that value. Yet when different parametrizations of the symmetry energy are explored in transport simulations, that pass near the asserted value, it is very hard to find sensitivity to the symmetry energy at $\rho \gtrsim \rho_0$ in nearly any observable. One reason are low asymmetries for the nuclear systems as a whole, additionally depleted in the center of the matter due to migration of the asymmetry to the surface. There is some advantage in going to heavier systems, as surface to volume ratio

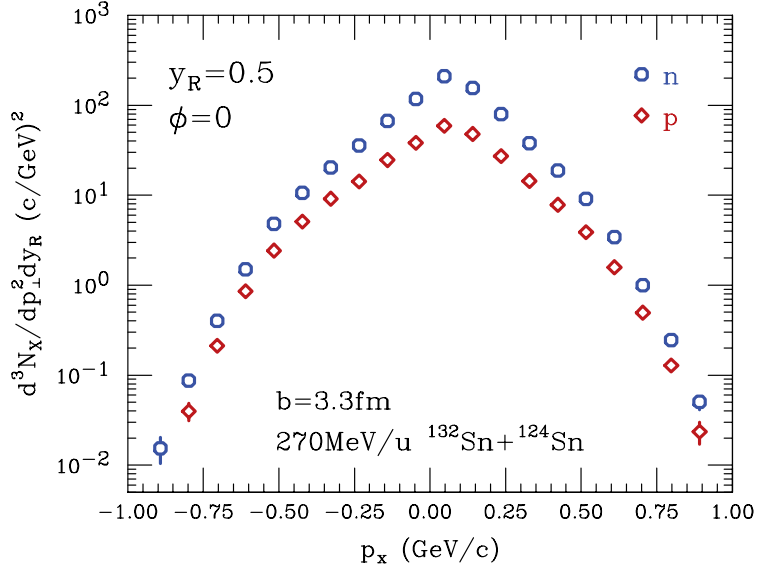


FIG. 6. Triple differential distributions in the reaction plane at $y_R = 0.5$, for neutrons (circles) and protons (diamonds), from the pBUU simulations of $^{132}\text{Sn} + ^{124}\text{Sn}$ collisions at 270 MeV/nucl and $b = 3.3$ fm. The rapidity y_R is here in the nucleon-nucleon center of mass and normalized to the beam.

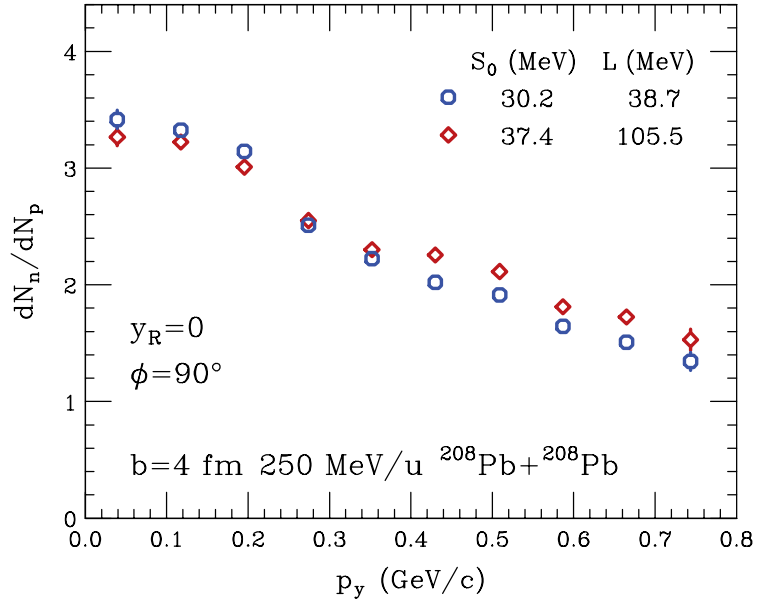


FIG. 7. Ratio of neutron yield to proton yield in 250 MeV/nucl $^{208}\text{Pb} + ^{208}\text{Pb}$ collisions at $b = 4$ fm, at midrapidity, in the direction perpendicular to the reaction plane, as a function of transverse momentum. The two symbol sets represent the results for two different parametrizations of symmetry energy: diamonds - stiff with $L = 105.5$ MeV and circles - moderately soft with $L = 38.7$ MeV. The two parametrizations are chosen so that they yield the symmetry energy at $\rho \sim 2\rho_0/3$ consistent with the conclusions from binding energies of heavy nuclei and other determinations pertaining to subnormal densities.

drops and Coulomb interactions help to maintain significant interior asymmetry, both in the initial state and in reaction dynamics [19]. Access to the 3D information should help too. Indeed, if one examines nucleonic spectra in direction perpendicular to the reaction plane, in 250 MeV/nucl $^{208}\text{Pb} + ^{208}\text{Pb}$ collisions at $b = 4$ fm, at $y_R = 0$, see Fig. 7, one can observe definite changes in the ratio of neutron to proton yields, when the symmetry energy evolves from moderately soft to stiff, with its slope parameter at ρ_0 changing from $L = 38.7$ MeV to $L = 105.5$ MeV. Both parametrizations of the symmetry pass by the consensus value at $\rho \sim 2\rho_0/3$.

The fact that a stiff symmetry energy raises the neutron-proton ratio at high transverse momentum agrees with intuitive expectations. However, the fact that it lowers the ratio at low momenta is somewhat surprising. Likely the

unexpected features of both Figs. 6 or 7 are tied to evolution of particle emission with time. The ratio being higher than the overall for the system of 1.54 in Fig. 7, for most transverse momenta, irrespective of the EOS, may be due to Coulomb interactions that push protons out not only in the transverse directions, but also along the beam axis.

In practical comparisons of transport theory to data it is common to make sure that many more rudimentary aspects of the data are understood on equal footing with those more sophisticated. I.e., other aspects of measured and calculated distributions would need to be simultaneously checked and more calculations would need to be carried out, than here, to draw credible physics conclusions.

V. CONCLUSIONS

We put forward the proposition to apply deblurring, borrowed from optics, to nuclear observables affected by uncertainty in the reaction plane determination. The central-limit yields the blurring function relatively faithfully for as few particles as 10 in an event (the 1D schematic case is operationally equivalent to that for the reaction plane), exploiting just few basic averages for the events. Ultimately, though, a simulation may be employed, self-consistent with the deblurring. The deblurring, such as with the Richardson-Lucy method, can work locally in the azimuthal angle only improving the 3D characteristics of collision events that are already resolved to some extent with the estimated reaction plane. This is a potential improvement over the complete Fourier decomposition of 3D characteristics in the azimuth. Importantly, estimation of the reaction plane can be made with particles measured in a different detector than the one used to detect the particle or particles for which the 3D characteristics are desired.

In actual data analysis, other correlations than those associated with the reaction plane will be present in the final states, in particular tied to the total momentum conservation, interactions at low relative velocity and sequential decays. Strategies to deal with these have been developed in other contexts [5, 12] and first the base needs to be established ignoring these correlations, which has been attempted here. Detector inefficiencies will need to be dealt with and interestingly those can be incorporated into the RL method as formulated in Sec. II. Going farther, hopefully the deblurring might be applied to nuclear detectors, in no connection to the reaction plane, just as it is applied to the optical instruments.

Finally, we hope that the deblurring, revealing 3D distributions, could help extract novel physics information from the heavy-ion collisions, that we tried to illustrate. Beyond single-particle distributions tied to the reaction plane, we hope that the strategy could be used for low-velocity correlations [20].

ACKNOWLEDGMENTS

The authors benefited from discussions with Scott Pratt and with members of the $S\pi RIT$ Collaboration. This work was supported by the U.S. Department of Energy Office of Science under Grant DE-SC0019209.

[1] P. Danielewicz and G. Odyniec, Physics Letters B **157**, 146 (1985), LBL Report 18600 (1984).

[2] M. Demoulin, D. L'Hôte, J. P. Alard, J. Augerat, R. Babinet, N. Bastid, F. Brochard, C. Cavata, N. De Marco, P. Dupieux, H. Fanet, Z. Fodor, L. Fraysse, P. Gorodetzky, J. Gosset, T. Hayashino, M. C. Lemaire, A. Le Merby, B. Lucas, J. Marroncle, G. Montarou, M. J. Parizet, J. Poitou, C. Racca, W. Schimmerling, Y. Terrien, and O. Valette, Physics Letters B **241**, 476 (1990); M. Demoulin, *Collective Flow Studies in Central Collisions Between Nuclei at Several Hundreds of MeV per Nucleon*, Ph.D., L'Universite de Paris-Sud, Orsay (1989), Report CEA-N-2628.

[3] S. Voloshin and Y. Zhang, Zeitschrift für Physik C Particles and Fields **70**, 665 (1996).

[4] A. M. Poskanzer and S. A. Voloshin, Physical Review C **58**, 1671 (1998).

[5] HADES Collaboration, J. Adamczewski-Musch, O. Arnold, C. Behnke, A. Belouinna, A. Belyaev, J. Berger-Chen, A. Blanco, C. Blume, M. Böhmer, P. Bordalo, S. Chernenko, L. Chlad, I. Ciepal, C. Deveaux, J. Dreyer, E. Epple, L. Fabbietti, O. Fateev, P. Filip, P. Fonte, C. Franco, J. Friese, I. Fröhlich, T. Galatyuk, J. Garzón, R. Gernhäuser, O. Golosov, M. Golubeva, R. Greifenhagen, F. Guber, M. Gumberidze, S. Harabasz, T. Heinz, T. Hennino, S. Hlavac, C. Höhne, R. Holzmann, A. Ierusalimov, A. Ivashkin, B. Kämpfer, T. Karavicheva, B. Kardan, I. Koenig, W. Koenig, M. Kohls, B. Kolb, G. Korcyl, G. Kornakov, F. Kornas, R. Kotte, A. Kugler, T. Kunz, A. Kurepin, A. Kurilkin, P. Kurilkin, V. Ladygin, R. Lalik, K. Lapidus, A. Lebedev, L. Lopes, M. Lorenz, T. Mahmoud, L. Maier, A. Malige, M. Mamaev, A. Mangiarotti, J. Markert, T. Matulewicz, S. Maurus, V. Metag, J. Michel, D. Mihaylov, S. Morozov, C. Müntz, R. Münzer, L. Naumann, K. Nowakowski, Y. Parpottas, V. Pechenov, O. Pechenova, O. Petukhov, K. Piasecki, J. Pietraszko, W. Przygoda, K. Pysz, S. Ramos, B. Ramstein, N. Rathod, A. Reshetin, P. Rodriguez-Ramos, P. Rosier, A. Rost, A. Rustamov, A. Sadovsky, P. Salabura, T. Scheib, H. Schuldes, E. Schwab, F. Scozzi, F. Seck, P. Sellheim, I. Selyuzhenkov, J. Siebenson, L. Silva, U. Singh, J. Smyrski, Y. Sobolev, S. Spataro, S. Spies, H. Ströbele, J. Stroth, C. Sturm, O. Svoboda, M. Szala,

P. Tlusty, M. Traxler, H. Tsertos, E. Usenko, V. Wagner, C. Wendisch, M. Wiebusch, J. Wirth, D. Wójcik, Y. Zanevsky, and P. Zumbruch, *Physical Review Letters* **125**, 262301 (2020).

[6] F. Vankawala, A. Ganatra, and A. Patel, *International Journal of Computer Applications* **116**, 15 (2015).

[7] W. H. Richardson, *Journal of the Optical Society of America* **62**, 55 (1972).

[8] L. B. Lucy, *The Astronomical Journal* **79**, 745 (1974).

[9] S. Remmelle and J. Hesser, in *Bildverarbeitung für die Medizin 2009*, Informatik aktuell, edited by H.-P. Meinzer, T. M. Deserno, H. Handels, and T. Tolxdorff (Springer, Berlin, Heidelberg, 2009) pp. 400–404.

[10] N. Dey, L. Blanc-Feraud, C. Zimmer, P. Roux, Z. Kam, J.-C. Olivo-Marin, and J. Zerubia, *Microscopy Research and Technique* **69**, 260 (2006).

[11] A. Andronic, J. Lukasik, W. Reisdorf, and W. Trautmann, *The European Physical Journal A - Hadrons and Nuclei* **30**, 31 (2006).

[12] P. Danielewicz, H. Ströbele, G. Odyniec, D. Bangert, R. Bock, R. Brockmann, J. W. Harris, H. G. Pugh, W. Rauch, R. E. Renfordt, A. Sandoval, D. Schall, L. S. Schroeder, and R. Stock, *Physical Review C* **38**, 120 (1988).

[13] W. Reisdorf, A. Andronic, R. Averbeck, M. L. Benabderrahmane, O. N. Hartmann, N. Herrmann, K. D. Hildenbrand, T. I. Kang, Y. J. Kim, M. Kiš, P. Koczoń, T. Kress, Y. Leifels, M. Merschmeyer, K. Piasecki, A. Schüttauf, M. Stockmeier, V. Barret, Z. Basrak, N. Bastid, R. Ćaplar, P. Crochet, P. Dupieux, M. Dželalija, Z. Fodor, P. Gasik, Y. Grishkin, B. Hong, J. Kecskemeti, M. Kirejczyk, M. Korolija, R. Kotte, A. Lebedev, X. Lopez, T. Matulewicz, W. Neubert, M. Petrovici, F. Rami, M. S. Ryu, Z. Seres, B. Sikora, K. S. Sim, V. Simion, K. Siwek-Wilczyńska, V. Smolyankin, G. Stoica, Z. Tymiński, K. Wiśniewski, D. Wohlfarth, Z. G. Xiao, H. S. Xu, I. Yushmanov, and A. Zhilin, *Nuclear Physics A* **848**, 366 (2010).

[14] P. Danielewicz, *Physical Review C* **51**, 716 (1995).

[15] P. Danielewicz, *Nuclear Physics A* **673**, 375 (2000).

[16] H. Wolter *et al.* (2021), to be submitted for publication.

[17] G. Jhang, J. Estee, J. Barney, G. Cerizza, M. Kaneko, J. W. Lee, W. G. Lynch, T. Isobe, M. Kurata-Nishimura, T. Murakami, C. Y. Tsang, M. B. Tsang, R. Wang, D. S. Ahn, L. Atar, T. Aumann, H. Baba, K. Boretzky, J. Brzychczyk, N. Chiga, N. Fukuda, I. Gasparic, B. Hong, A. Horvat, K. Ieki, N. Inabe, Y. J. Kim, T. Kobayashi, Y. Kondo, P. Lasko, H. S. Lee, Y. Leifels, J. Lukasik, J. Manfredi, A. B. McIntosh, P. Morfouace, T. Nakamura, N. Nakatsuka, S. Nishimura, R. Olsen, H. Otsu, P. Pawłowski, K. Pelczar, D. Rossi, H. Sakurai, C. Santamaria, H. Sato, H. Scheit, R. Shane, Y. Shimizu, H. Simon, A. Snoch, A. Sochocka, Z. Sosin, T. Sumikama, H. Suzuki, D. Suzuki, H. Takeda, S. Tangwancharoen, H. Ternqvist, Y. Togano, Z. G. Xiao, S. J. Yennello, J. Yurkon, Y. Zhang, M. Colonna, D. Cozma, P. Danielewicz, H. Elfner, N. Ikeno, C. M. Ko, J. Mohs, D. Oliynychenko, A. Ono, J. Su, Y. J. Wang, H. Wolter, J. Xu, Y.-X. Zhang, and Z. Zhang, *Physics Letters B* **813**, 136016 (2021).

[18] W. G. Lynch and M. B. Tsang, arXiv:2106.10119 [astro-ph, physics:nucl-ex, physics:nucl-th] (2021).

[19] J. R. Stone, P. Danielewicz, and Y. Iwata (2021), to be submitted for publication.

[20] M. A. Lisa, N. N. Ajitanand, J. M. Alexander, M. Anderson, D. Best, F. P. Brady, T. Case, W. Caskey, D. Cebra, J. L. Chance, P. Chung, B. Cole, K. Crowe, A. C. Das, J. E. Draper, M. L. Gilkes, S. Gushue, M. Heffner, A. S. Hirsch, E. L. Hjort, L. Huo, M. Justice, M. Kaplan, D. Keane, J. C. Kintner, J. Klay, D. Krofcheck, R. A. Lacey, J. Lauret, H. Liu, Y. M. Liu, R. McGrath, Z. Milosevich, G. Odyniec, D. L. Olson, S. Y. Panitkin, C. Pinkenburg, N. T. Porile, G. Rai, H. G. Ritter, J. L. Romero, R. Scharenberg, L. Schroeder, B. Srivastava, N. T. B. Stone, T. J. M. Symons, R. Wells, J. Whitfield, T. Wienold, R. Witt, L. Wood, and W. N. Zhang, *Physics Letters B* **496**, 1 (2000).